The bifurcation of the unstable periodic orbits in bounded and unbounded three-disk billiards

1994 J. Phys. A: Math. Gen. 27 4791

(http://iopscience.iop.org/0305-4470/27/14/010)

J. Phys. A: Math. Gen. 27 (1994) 4791–4803. Printed in the UK

The bifurcation of the unstable periodic orbits in bounded and unbounded three-disk billiards

Mitsusada M Sano

Department of Applied Physics, Tokyo Institute of Technology, Oh-okayama, 2-12-10, Meguro, 152, Tokyo, Japan

Received 18 February 1994, in final form 5 May 1994

Abstract. The bifurcation of unstable periodic orbits (UPOs) in bounded and unbounded billiards are investigated. The billiard systems studied in this paper consist of three disks and have C_{3v} symmetry. It is found numerically that these systems have essentially two different types of bifurcation for changing the structure of the UPOs. The first type of bifurcation is caused by the tangential collision of the trajectory with a convex boundary segment. The second type of bifurcation is caused by the collision of the trajectory with a vertex point, where two smooth boundary segments meet at a finite angle. The vertex points on the boundary play the central geometrical role of organizing the UPOs in these billiard systems.

1. Introduction

In recent years, increasing efforts have been made to understand the organization of unstable periodic orbits (UPOs) in classical chaotic systems [1]. The importance of UPOs is very clear when we remember that the UPOs of a classical system serve as the bone structure of the flow in phase space.

Mathematically, if the system is hyperbolic, many important characteristic quantities, including the Hausdorff dimension of the invariant set, the Lyapunov exponent and the decay rate of the correlation function, can be calculated from information on the UPOs alone by using Ruelle's dynamical zeta function [2]. Furthermore, the bone structure built by UPOs essentially governs the dynamics of not only the classical system but also the corresponding quantum system through the classical–quantum correspondence principle. Nowadays, this is very apparent from the success of the semiclassical quantization theory developed by Gutzwiller [3] which enables us to calculate the quantum energy levels from the classical UPOs.

In order to clearly understand the bone structure woven by the UPOs, many idealized hyperbolic systems have been investigated. These include the cat map [4], the baker map [5], the three-disk system [6–9] and so on. Among these idealized systems, the three-disk system is the most suitable for our study towards a clearer understanding of the classical–quantum correspondence in chaotic systems, since this system does not have the number-theoretic anomalies which are observed in other systems such as the cat map. Accordingly, we choose the three-disk system as our model system and study, in this paper, the symbolic dynamics of the system which is the essence of the classical dynamics necessary for the semiclassical quantization. In particular, we concentrate our attention on the change in symbolic dynamics and its implication to the corresponding quantum dynamics when a system parameter is varied.

0305-4470/94/144791+13$19.50

This paper is organized in the following way. In section 2, two mathematical tools, which are used later, are explained. One is the symmetry reduction, which gives us a simplified description of a system that has some symmetry and the other is Birkhoff's method for locating many-periodic orbits. In section 3, after the symbolic dynamics for the three-disk billiards with C_{3v} symmetry is introduced, the bifurcation of the UPOs when the system parameter is varied is investigated for the unbounded three-disk billiards. In section 4, the bifurcation of UPOs is investigated for the bounded three-disk billiards and a new type of bifurcation is found. Furthermore, the change in the contribution of the UPOs to the zeta functions alters in these bifurcation processes is revealed. Finally, in section 5, we summarize the results obtained in this paper.

2. Methods

Let us explain our three-disk system. It consists of three disks of equal radius a located apart from each other by the same interdisk distance R and has the discrete symmetry C_{3v} (see figure 1). In addition to this geometrical symmetry, the dynamics of the system also has a kinematic symmetry in the time evolution, which will be explained below and in the appendix. (i) The former symmetry enables us to perform so-called *symmetry reduction* to contract the phase-space without loss of information. (ii) The latter symmetry allows us to use Birkhoff's method of symmetry lines to easily locate many-periodic orbits [10, 11].

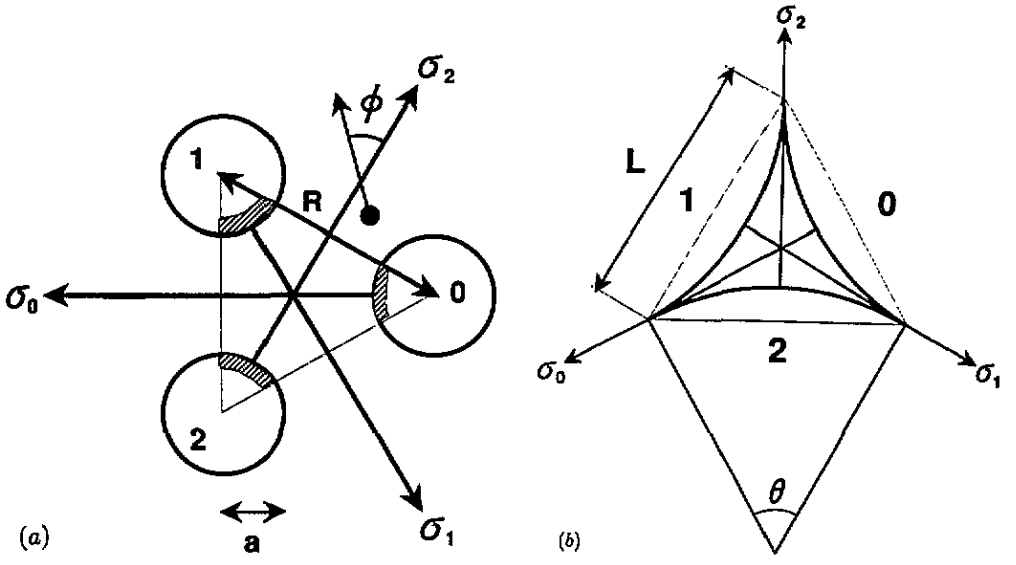

Figure 1. The model systems. (*a*) Unbounded three-disk system. The system parameter is the interdisk distance R ($R > 2$). The radius a is fixed at 1. (*b*) Bounded three-disk system. $\theta = t\pi/3$. The system parameter t for $0 \leqslant t \leqslant 1$ is related to the curvature of the disks, since L is fixed at 1.

Thanks to the symmetry reduction, we choose the symmetry lines instead of the usual boundary surfaces on the disks as a Poincaré section [11]. All symmetry lines are identified as a single Poincaré section $\mathcal{P}$ (symmetry reduction). A trajectory consists of a finite or

an infinite number of straight-line segments, which are called *paths*, between successive collisions on the disk boundaries. At the crossing point of the trajectory on the Poincaré section, the location in phase-space is specified by a pair of variables $(r, \cos\phi)$ where r is the one-dimensional coordinate along the symmetry line and ϕ is the angle between the direction of the trajectory and that of the symmetry line. Let T denote the return map on the Poincaré section $\mathcal{P}$; the phase point $(r, \cos\phi) \in \mathcal{P}$ at a crossing point is mapped to the phase point $T(r, \cos\phi) = (r', \cos\phi') \in \mathcal{P}$ at the next crossing point.

Next, we apply Birkhoff's method of symmetry lines to our system in order to find many-periodic orbits in the system. Birkhoff's method requires that the time-evolution operator T is represented as the product of two involution operators I_0 and I_1, namely

$$T = I_1 \circ I_0 \tag{1}$$

and

$$I_0^2 = I_1^2 = e \tag{2}$$

where e is the identity (see appendix and [10]). When a system has C_{3v} symmetry, the two operators I_0 and I_1 defined by

$$I_0(r, \cos\phi) \equiv (r, -\cos\phi) \tag{3}$$

and

$$I_1 \equiv T \circ I_0 \tag{4}$$

satisfy the above requirement [11]. Using these operators, we define the symmetry line $\mathcal{R}_n$, which is the invariant set after a time evolution of n steps following the operation I_0, by

$$\mathcal{R}_n \equiv \{r \in \mathcal{P};\, T^n \circ I_0\, r = r\} \tag{5}$$

for any integer n. These sets $\mathcal{R}_n$ can be obtained very easily in our numerical calculation due to the non-trivial relations

$$\mathcal{R}_{2n} = T^n \mathcal{R}_0 \tag{6}$$

$$\mathcal{R}_{2n+1} = T^n \mathcal{R}_1 \tag{7}$$

which are derived in the appendix for the reader's convenience. Finally, Birkhoff's argument tells us that the intersection $\mathcal{R}_m \cap \mathcal{R}_n$ includes (usually, a large number of) periodic points with period $|m-n|$, although some periodic points with the same period cannot be captured by the method in general.

3. Unbounded systems

Let the radius a of the disks be fixed at 1 and let the interdisk distance R as the system parameter vary. First, we consider the case for $R > 2$. In this case, the system is called *unbounded* since some trajectories escape to infinity.

Let us visualize Smale's horseshoe dynamics for the unbounded three-disk system (figure 2(*a*)). Since our final concern is the structure of the UPOs, there is no need to

inspect escape trajectories. Accordingly, we take the set of all trajectories which run from the hatched part of the boundary of a disk to that of another disk in figure 1(*a*) as the initial set $\Pi_0 \subset \mathcal{P}$ of trajectories for time evolution. (Other trajectories escape eventually.) The n-times iterated set Π_n is defined by $\Pi_n = T^n\Pi_0$. In figure 2, we depict Π_n for $n = -2, -1, 0, 1, 2$. The set Π_1 consists of two connected components, which are stripes stretched along the expanding direction and shrunk along the contracting direction. We remark that each connected component transversally intersects the initial set Π_0 along the expanding direction. Consequently, for any large positive n, the n-times iterated set Π_n transversally intersects Π_0 again. The same argument also holds for the transversality of Π_n ($n < 0$) along the contracting direction. Thus, for $m < 0$ and $n > 0$, any connected component of Π_m and any connected component of Π_n have a non-empty intersection. The horseshoe dynamics which satisfies this condition is called *complete*. It can be proved that the condition is equivalent to the grammar of the symbolic dynamics imposing no restriction on the Markov chain. The horseshoe dynamics which is not complete is called *incomplete*.

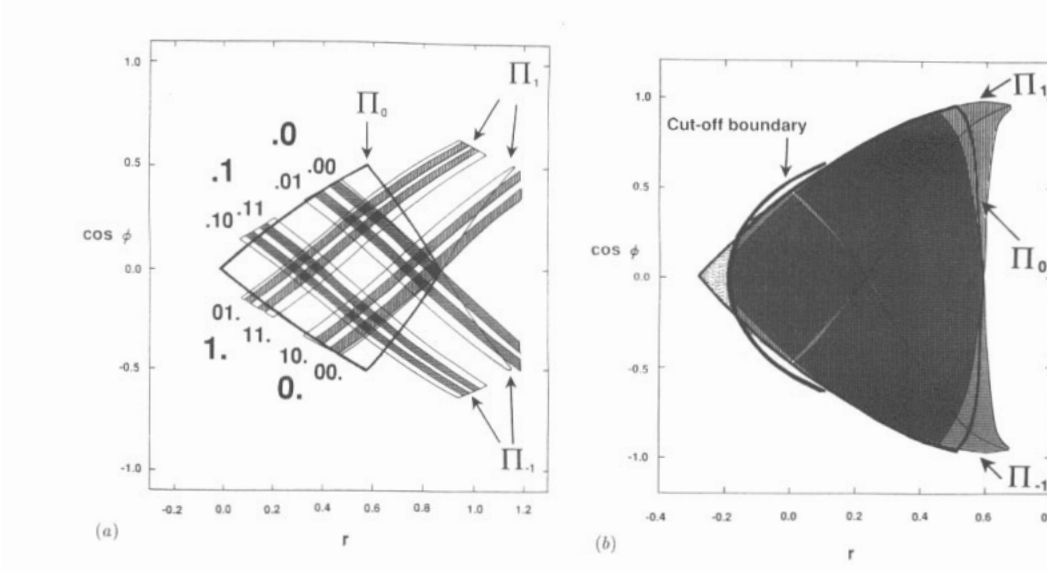

Figure 2. The forward and backward time evolution of the initial set Π_0 for the unbounded system. The set Π_n is the time-evolved set at the time step n. The initial set Π_0 is enclosed by the full curve. (*a*) $R = 3.0$. Π_ns are drawn for $n = -2, -1, 0, 1, 2$. Π_{-2} and Π_2 are hatched with horizontal and vertical lines, respectively. (*b*) $R = 2.048$. Π_ns are drawn for $n = -1, 0, 1$. Π_{-1} and Π_1 are hatched with horizontal and vertical lines, respectively. The dotted area stands for the unphysical region cut off by the eclipse.

As is seen in figure 2(*a*), after a time evolution of one step, the initial set Π_0, which is connected, splits into two connected components of Π_1. Let these two components of Π_1 be labelled by the symbols 0 and 1. The component labelled by 0 corresponds to the set of trajectories which reach, after a time evolution of one step, the same symmetry line from which the trajectories started at the initial time. On the other hand, the trajectories corresponding to the component labelled by 1 cross a different symmetry line. When the time evolution advances one step further, each component $s_1 \in \{0, 1\}$ of Π_1 splits again into two connected components $s_1 0$ and $s_1 1$ of Π_2. By repeating this procedure, each of the 2^n connected components of the n-times iterated set Π_n is labelled by a symbol sequence $s_1 s_2 \ldots s_n \in \{0, 1\}^n$. The same procedure is also applied for the backward time evolution

to the past. For $m < 0$, a connected component of the m-iterated set Π_m is labelled by $s_m \ldots s_{-2}s_{-1} \in \{0, 1\}^{|m|}$. Now, the intersection between the above two components of Π_m and Π_n is a small rectangle labelled by $s_m \ldots s_{-2}s_{-1} \cdot s_1 s_2 \ldots s_n$, where '$\cdot$' represents the origin of time. We can prove that the intersection shrinks to a point in the limit $m \to -\infty$ and $n \to \infty$. Consequently, each trajectory in the original dynamics corresponds to a unique bi-infinite symbol sequence. In this way, the symbolic dynamics is constructed. For $R > R_{c1} = 4/\sqrt{3} = 2.309\,401\ldots$, any path connecting two disks in the previous sense cannot be obstructed by the third disk; namely, an eclipse never occurs†.

Let us decrease the interdisk distance R to observe the bifurcation process. In figure 2(b), Π_n ($n = -1, 0, 1$) for $R = 2.048$ are depicted in the same way as before. We notice that each component of Π_n in figure 2(b) is fatter and has a rounder boundary curve compared with those in figure 2(a). Furthermore, the transversality for Π_ns breaks down in figure 2(b) as explained below. Thus, the horseshoe dynamics is now incomplete. The breakdown of the transversality is easily understood by drawing the cut-off boundary for physically-realizable trajectories in $\mathcal{P}$. The cut-off boundary in $\mathcal{P}$ corresponds to the trajectories which start from initial disks and tangentially touch other disks at the next collision after 1 step when the trajectories have evolved either forward or backward in time. (The appearance of such a cut-off boundary was studied in an 'abstract' scattering problem by Troll [13].) Accordingly, in figure 2(b), the dotted area in the left-hand side of the cut-off boundary corresponds to the unphysical trajectories which are obstructed by the eclipse by the third disk before reaching the destination disk. Of course, the symbol sequences corresponding to these unphysical trajectories are naturally unallowed. Since we are interested in physical UPOs and the unphysical area on $\mathcal{P}$ created by the eclipse may not contain any UPOs, a further detailed investigation to judge whether some original UPOs become unallowed in figure 2(b) is required. Consequently, we need a further detailed investigation to judge whether some UPOs are pruned in figure 2(b). Actually, it was found by Hansen [14] that by calculating when the outermost homoclinic point crosses the time-evolved cut-off boundary by some steps, unallowed symbol sequences appear when $R \leqslant R_{c2} = 2.048\,214\,19\ldots$. Such a system having unallowed symbol sequences is called *pruned*. We now know that our system is pruned since $R = 2.048$.

In order to visualize how the periodic orbits in $\mathcal{P}$ move and disappear when R is changed, we draw symmetry lines $\mathcal{R}_n$ on $\mathcal{P}$ in figure 3; (a)–(c) and (d)–(e) correspond to $R = 2.03$ and 2.01, respectively. In figure 3(a), $\mathcal{R}_1$ has two branches. One branch includes the fixed point of the map T corresponding to the symbol sequence $\ldots 0000\ldots \equiv \overline{0}$. (The overbar $\overline{ab\ldots z}$ stands for the infinite repetition $\ldots ab\ldots zab\ldots z\ldots$.) The other branch includes the fixed point of T corresponding to the symbol sequence $\overline{1}$. We denote the former branch as $\mathcal{R}_1^\tau$ and the latter branch as $\mathcal{R}_1^\sigma$. We also denote the iterated sets of $\mathcal{R}_1^\sigma$ and $\mathcal{R}_1^\tau$ as $\mathcal{R}_{2n+1}^\sigma = T^n\mathcal{R}_1^\sigma$ and $\mathcal{R}_{2n+1}^\tau = T^n\mathcal{R}_1^\tau$, respectively, and the union of the two sets as $\mathcal{R}_{2n+1} = \mathcal{R}_{2n+1}^\tau \cup \mathcal{R}_{2n+1}^\tau$ (see equation (7)). Remember that the crossing point between two symmetry lines is a periodic point.

Note what happens to the crossing points between the symmetry lines when the system parameter R is changed. The same symmetry lines are drawn in the area close to the cut-off boundary in figures 3(b) and (d), which correspond to $R = 2.03$ and 2.01, respectively. We notice that several crossing points, marked by the star in (b), disappear in (d) since each symmetry line in (b) is scraped in (d) by the unphysical area to become shorter and unable to have a crossing point with another symmetry line. This is one way for the crossing

† When this condition is satisfied, it is mathematically proved that the correspondence between the subshift of finite type on the symbol sequences and the original dynamics for non-escaping trajectories is perfect and the topological entropy for the original dynamics surely exists [12].

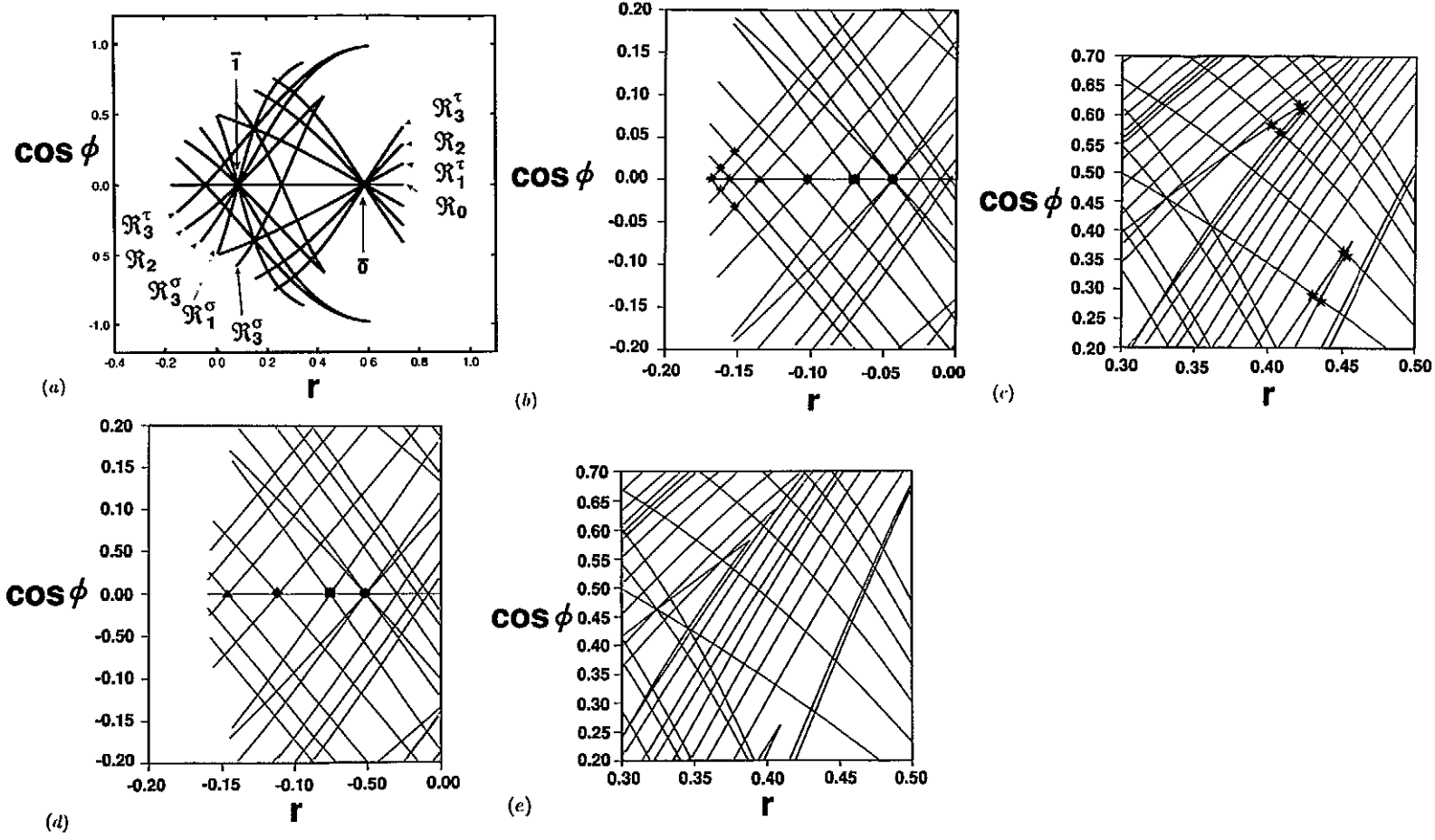

Figure 3. The backward and forward time evolution of the symmetry lines $\mathcal{R}_n$ on the Poincaré section for the unbound system. (*a*) $R = 2.03$, $\mathcal{R}_n$ for $|n| \leqslant 3$, overall figure; (*b*) $R = 2.03$, $\mathcal{R}_n$ for $|n| \leqslant 7$, magnification near the cut-off boundary; (*c*) $R = 2.03$, $\mathcal{R}_n$ for $|n| \leqslant 7$, magnification near the wedge; (*d*) $R = 2.01$, $\mathcal{R}_n$ for $|n| \leqslant 7$, the same area as (*b*) near the cut-off boundary; (*e*) $R = 2.01$, $\mathcal{R}_n$ for $|n| \leqslant 7$, the same area as (*c*) near the wedge. In (*b*) and (*d*), the crossing points corresponding to the same sequence are marked with an identical symbol (●, ■, ♦ or ▲). In (*b*) and (*c*), the crossing points which disappear in (*d*) and (*e*), respectively, are marked by ★.

points to disappear in the parameter change. There is another way for the crossing points to disappear. In figures 3(*c*) and (*e*), some symmetry lines in another area are drawn similarly for $R = 2.03$ and 2.01, respectively. In these figures, several symmetry lines are folded back at the wedge-shaped corners. We observe that when R is changed, these wedges move and some of them lose the crossing points with other transversal symmetry lines. See the crossing points marked with a star in (*c*). These two ways for crossing points (i.e. periodic points) to disappear in the parameter change originate from a common mechanism; the tangential touch of an orbit with the boundary of an obstructive disk. Accordingly, we call this bifurcation mechanism *tangential-type bifurcation*. The periodic points near the cut-off boundary in figure 3(*b*) no longer exist in figure 3(*d*). This means that the horseshoe is scraped by the cut-off boundary in figure 3(*d*). By exploring the symbol sequences corresponding to the periodic points on the straight line $\cos\phi = 0$ which are scraped in the process, we can find the ordering rule for symbol sequences, of the form $\overline{10^n1}$ with $n \geqslant 1$, to disappear in the process; a symbol sequence $\overline{10^n1}$ with larger n disappears earlier. On the other hand, a consideration based upon the symmetry of the system and the correspondence between the Poincaré section and the space of symbol sequences tells us that the above family contains the symbol sequence pruned earliest in the process. Consequently, the first symbol sequence which becomes forbidden in the process is $\ldots 001.100\ldots$. This symbol sequence corresponds to the left-outermost homoclinic point on the Poincaré section which originates from the fixed point $\overline{0}$.

4. Bounded systems

Bounded three-disk billiard systems have been studied by several authors [14, 15]. In order to understand the mechanism of pruning in bounded systems, we continue to study the same three-disk system for $R \leqslant 2$. First, we introduce a new variable t to replace R as the system parameter. The variable t is defined in such a way that the centre angle of each arc in figure 1(*b*) is $t\pi/3$ ($0 \leqslant t \leqslant 1$). For $t = 0$, the shape of our billiard becomes an equilateral triangle and its dynamics becomes integrable. For $t = 1$, each pair of two arcs meet tangentially at the vertex. As explained before, our system now has pruned symbolic dynamics. In figure 4, the time evolution of the symmetry lines is again depicted for two parameters $t = 1$ and $t = 0.3$. We observe that the periodic points disappear according to tangential-type bifurcation. Furthermore, we find another new bifurcation mechanism to erase periodic points which exists only when the system is bounded. When t decreases, a UPO falls into a vertex to disappear (figure 5(*b*1)–(*b*3)). We call this type of bifurcation *vertex-type bifurcation*. In general, if a system has a vertex point then this new bifurcation mechanism can take place in the system.

Next we show how the stability of the UPOs changes in the bifurcation processes. We define the stretching factor Λ as $\Lambda \equiv |\det(M - 1)|$ where M is the one-turn linearized Poincaré map around the UPOs. Roughly speaking, Λ is the amplification factor of a small initial deviation from the UPO after one turn. The stretching factor Λ of the UPOs (together with their action and period) is the essential quantity needed to characterize the classical dynamics and the semiclassical quantum dynamics. The classical and the semiclassical zeta functions are constructed from these quantities [2, 3] (to be precise, the semiclassical zeta functions require one more quantity, i.e. Maslov index.)

First, let us investigate the change in the stretching factor Λ of UPOs in tangential-type bifurcations. As found by Hansen [14], when a UPO disappears at a bifurcation point due to a tangential-type bifurcation, an infinite number of UPOs disappear simultaneously at the same

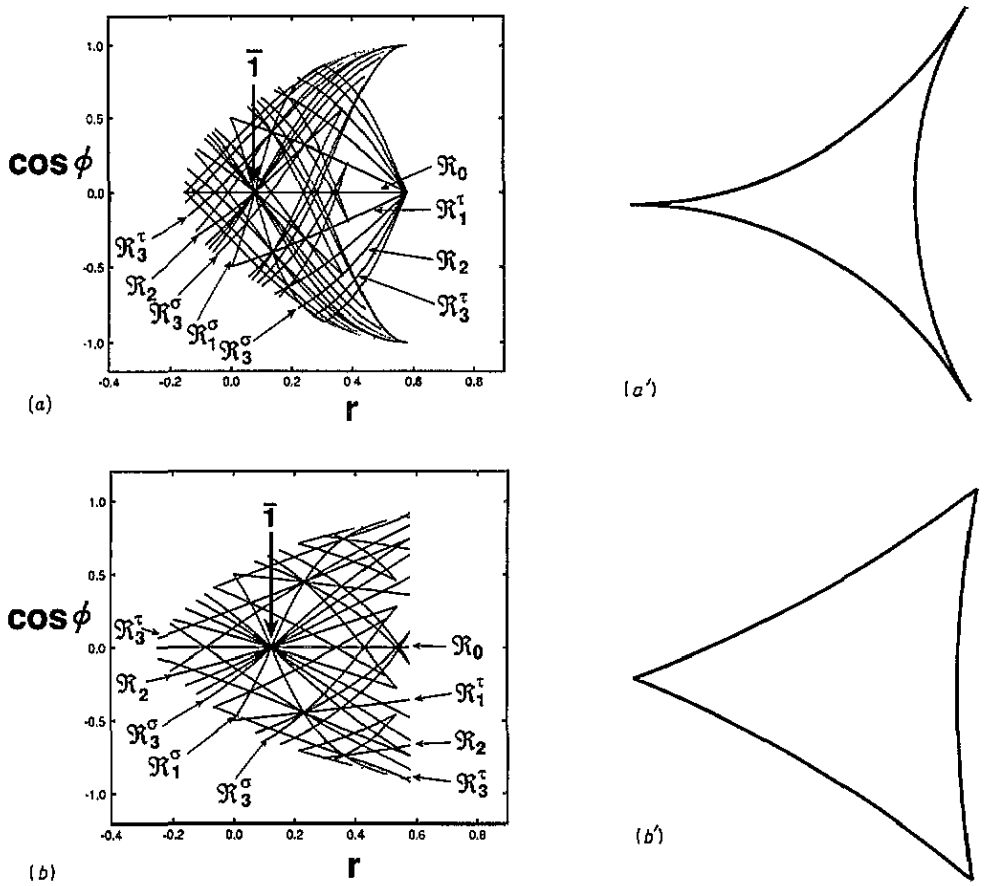

Figure 4. The forward and backward time evolution of the symmetry lines $\mathcal{R}_n$ on the Poincaré section for the bounded system. (*a*) $t = 1.0$, $\mathcal{R}_n$ for $|n| \leqslant 5$; (*b*) $t = 0.3$, $\mathcal{R}_n$ for $|n| \leqslant 5$. In (*a*) and (*b*), only $\mathcal{R}_n$s for $n = 0, 1, 2, 3$ are indicated. The shapes of the billiards for the parameters are shown in (*a'*) and (*b'*) respectively. In (*a'*), the arcs meet tangentially at vertices.

point. These UPOs form a family. The change in the stretching factor Λ as a function of the system parameter t is shown in figure 6(*a*) for two UPOs in the same family. In the figure, the vertical axis represents the inverse of Λ in log scale, since Λ^{-1} ($\Lambda^{-1/2}$) and its integer powers appear as the weighting factors of UPOs in the Ruelle zeta function (Gutzwiller zeta function). We find that when the parameter t changes, the UPO labelled $\overline{10001101}$ shows a slow change and the inverse of the stretching factor Λ remains at a finite value just before the bifurcation point although the UPO itself disappears abruptly at this point. Thus, the contribution of the present UPO has a discontinuous change at the bifurcation point. On the other hand, in figure 6(*a*), another UPO labelled $\overline{100001100}$ becomes more and more stable as the parameter t approaches the bifurcation point. At the bifurcation point, Λ diverges and the weight factor Λ^{-1} of the zeta functions vanishes. Namely, the transition is continuous. Consequently, discontinuous and continuous transitions coexist in the family of UPOs belonging to the same tangential-type bifurcation.

Furthermore, it is numerically confirmed that for any family of UPOs in the above sense, there exists only one UPO which exhibits a discontinuous transition and all the other infinite number of UPOs exhibit continuous transitions. Thus, the single UPO whose Λ^{-1} does not

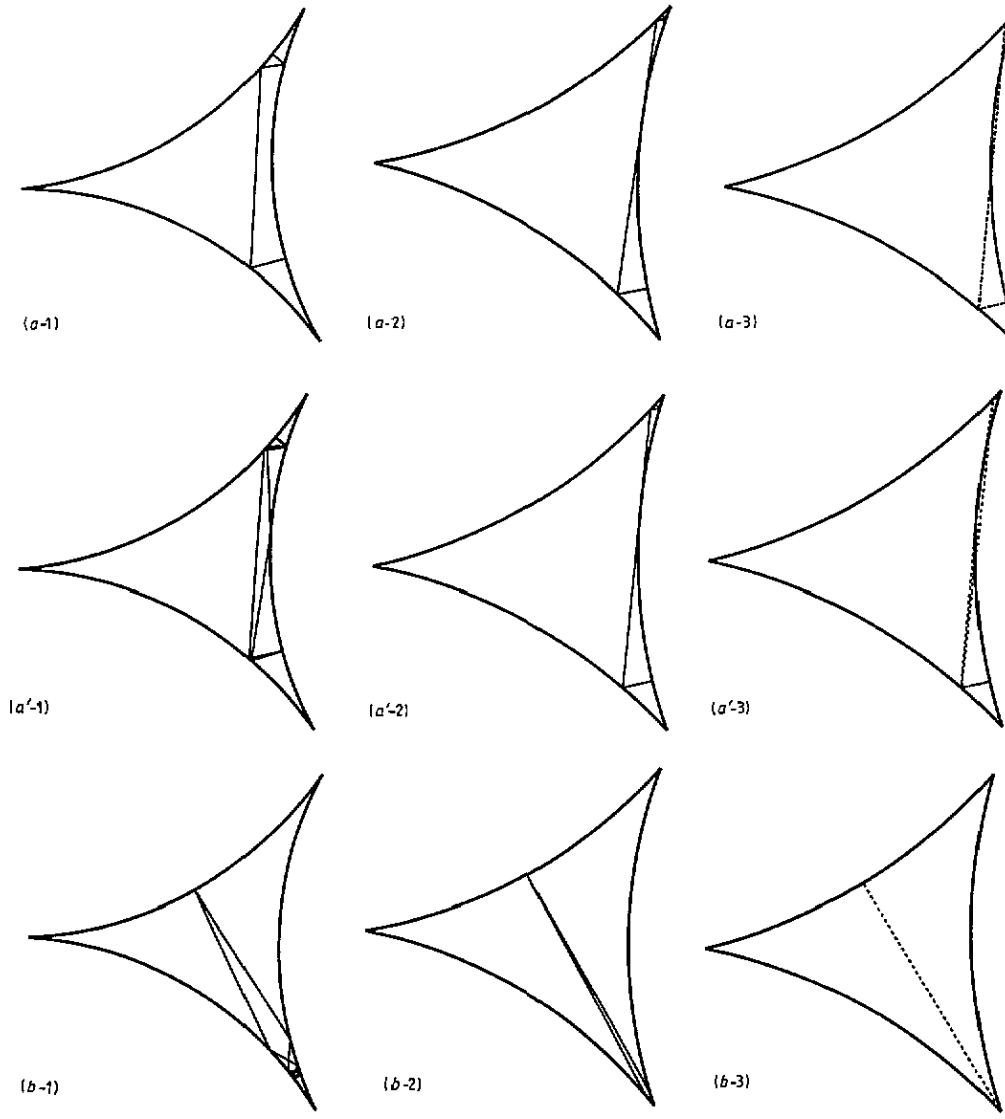

Figure 5. The bifurcations of UPOs in the bounded system when the system parameter t is varied. (How the contribution of these UPOs to the zeta functions changes in the bifurcation process is depicted in figure 6.) $(a1)$–$(a3)$ tangential-type bifurcation exhibiting discontinuous transition. The UPO which is self-retracing corresponds to the symbol sequence $\overline{10001101}$. The parameter values are $t = 0.9, 0.6176, 0.595$, respectively; $(a'1)$–$(a'3)$ tangential-type bifurcation exhibiting continuous transition. Similarly, for $\overline{100001100}$ and $t = 0.9, 0.6176, 0.58$. The UPOs in (a) and (a') belong to the same family to disappear simultaneously. Just on the bifurcation point $(a'2)$, the present UPOs degenerate with the UPOs in (a); $(b1)$–$(b3)$ vertex-type bifurcation. Similarly, for $\overline{100000011}$ and $t = 0.9, 0.652, 0.58$.

vanish at the bifurcation point completely dominates the change in the contribution to the zeta function from the whole family.

Second, the change in Λ^{-1} is calculated for the vertex-type bifurcation (figure 6(b)). Clearly, the UPOs exhibits a discontinuous transition. In our numerical experiments, all of the vertex-type bifurcations exhibit a discontinuous transition with no exceptions.

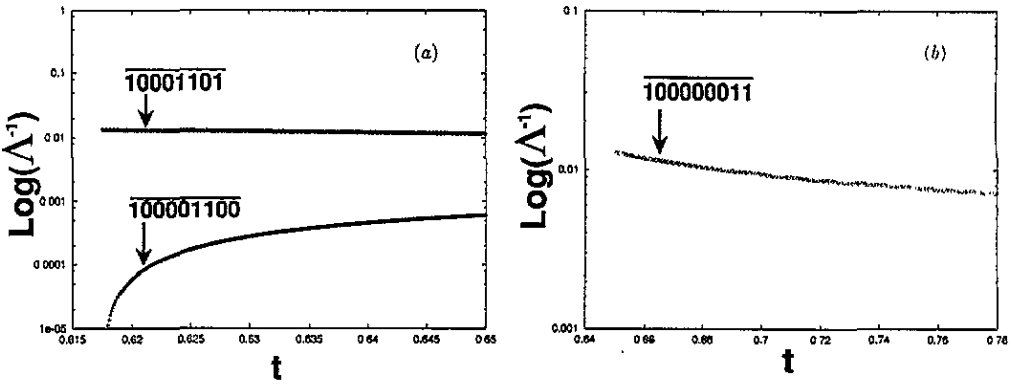

Figure 6. The change of the Λ^{-1} for the UPOs in the same bifurcations shown in figure 5 when the system parameter t is varied. (Λ is the stretching factor of the UPOs and Λ^{-1} represents the weight factor of the UPOs to contribute to the zeta functions.) (*a*) The tangential-type bifurcation. Two UPOs in the same family correspond to the symbol sequences $\overline{10001101}$ and $\overline{100001100}$. The contribution of the former UPOs to the zeta functions exhibits the discontinuous transition, whereas that of the latter exhibits the continuous transition. (It is found numerically that when a self-retracing UPO shows tangential-type bifurcation, the transition is always discontinuous.) (*b*) The vertex-type bifurcation. The UPOs correspond to the symbol sequence $\overline{100000011}$. The transition is discontinuous. (It is found numerically that any vertex-type bifurcation exhibits the discontinuous transition.)

5. Summary

We have reported the following two discoveries in the present paper: (i) there exists a new pruning mechanism for UPOs due to a vertex for bounded billiard systems; and (ii) the UPOs which are pruned at the same bifurcation point through a tangential-type bifurcation are classified into two categories. The first category consists of a single UPO whose Λ^{-1} remains finite at the bifurcation point, whereas the second category consists of an infinite number of UPOs for which the Λ^{-1} vanish at this point. A further study on the influence of the bifurcations on the zeta functions will be reported elsewhere [16].

Acknowledgments

The author would like to thank Professor K Kitahara, Professor Y Aizawa, Dr S Adachi, Dr A Shudo, Dr T Harayama, Y Shimizu and T Takami for useful discussions and continuous encouragement and also Dr P Gaspard for critical comments. In particular, the author thanks again Dr S Adachi for reading the manuscript during the preparation of this paper. While this paper was being refereed, the author received Dr K T Hansen's PhD thesis [17]. In this thesis, he investigated the vertex-(or corner-)type bifurcation and its symbolic dynamics in the integrable limit. The author is grateful to Dr K T Hansen for sending his unpublished PhD thesis [17]. The present work was carried out independently. This work was supported by Grant-in-Aids for Scientific Research from the Ministry of Education, Science and Culture of Japan.

Appendix. Birkhoff's method for finding periodic orbits

In this appendix, we explain Birkhoff's method for finding periodic orbits and derive the non-trivial relations (6) and (7) in section 2. Birkhoff's method is a way of determining the location of periodic orbits in the Poincaré section for a system which has some discrete symmetry [10, 11]. The required symmetry is that the discrete time evolution T (i.e. Poincaré map) is given as the product of two involutions

$$T = I_1 \circ I_0 \tag{A.1}$$

where

$$I_0 \circ I_0 = I_1 \circ I_1 = e \tag{A.2}$$

and e is the identity.

For billiard systems, if we take the velocity reverse operation as I_0, which is obviously an involution, it can be proved that the operator I_1, defined by $I_1 \equiv T \circ I_0$, is also an involution.

In particular, for two-dimensional billiards, the above statement is proved easily as follows. The dynamics for these systems can be represented in the so-called Birkhoff coordinates $(r, \sin\varphi)$ at the impact point on the boundary where r is the coordinate along the boundary and φ is the angle between the outgoing direction and the normal vector at the impact point. Accordingly, these variables take values in the range

$$(r, \sin\varphi) \qquad 0 \leqslant r < r_{\max} \qquad -\tfrac{1}{2}\pi \leqslant \varphi \leqslant \tfrac{1}{2}\pi \tag{A.3}$$

where $r_{\max}$ is the perimeter of the boundary. In this representation, the velocity reverse operation I_0 is expressed as

$$I_0 : (r, \sin\varphi) \mapsto (r, \sin(-\varphi)). \tag{A.4}$$

Suppose that a point $(r, \sin\varphi)$ in phase-space is mapped to $(r', \sin\varphi')$ and $(r'', \sin\varphi'')$ by the Poincaré map T and its inverse T^{-1}, respectively. Then $I_1 \equiv T \circ I_0$ is calculated as

$$\begin{aligned} I_1(r, \sin\varphi) &\equiv T \circ I_0(r, \sin\varphi) \\ &= T(r, \sin(-\varphi)) \\ &= (r'', \sin(-\varphi'')). \end{aligned} \tag{A.5}$$

By using (A.5), we now know that I_1 is an involution

$$\begin{aligned} I_1 \circ I_1(r, \sin\varphi) &= T \circ I_0 \circ T \circ I_0(r, \sin\varphi) \\ &= T \circ I_0(r'', \sin(-\varphi'')) \\ &= T(r'', \sin(\varphi'')) \\ &= (r, \sin\varphi). \end{aligned} \tag{A.6}$$

Finally, we will prove the non-trivial relations (6) and (7) used in section 2. We begin by extending the definition of I_1 to I_j for any $j \in Z$

$$I_j \equiv T^j \circ I_0. \tag{A.7}$$

By using (A.1) and (A.2), it is easily shown that I_j is also an involution

$$I_j \circ I_j = e. \tag{A.8}$$

Let us consider the algebra generated by the operator product on the set $\{T^k; k \in Z\} \cup \{I_j; j \in Z\}$. The set is closed under the product and becomes a group by itself, since

$$T^j \circ I_k = I_{j+k} \tag{A.9}$$

$$I_j \circ I_k = T^{j-k} \tag{A.10}$$

$$I_j \circ T^k = I_{j-k}. \tag{A.11}$$

These relations are obtained by using (A.1), (A.2), (A.7) and (A.8). We define the set of fixed points of the involution I_j as

$$\mathcal{R}_j \equiv \{r \in \mathcal{P}; I_j r = r\}. \tag{A.12}$$

By using (A.7)–(A.11), we get the following two relations:

$$T^n \mathcal{R}_k = \mathcal{R}_{2n+k} \tag{A.13}$$

$$I_n \mathcal{R}_k = \mathcal{R}_{2n-k}. \tag{A.14}$$

The derivations of (A.13) and (A.14) are as follows.

$$\begin{aligned} r \in \mathcal{R}_{2n+k} &\Leftrightarrow r = I_{2n+k} r \qquad \text{((A.12) is used)} \\ &= T^n \circ I_k \circ T^{-n} r \qquad \text{((A.9) and (A.11) are used)} \\ &\Leftrightarrow T^{-n} r = I_k \circ (T^{-n} r) \qquad (A.15) \\ &\Leftrightarrow T^{-n} r \in \mathcal{R}_k \qquad \text{((A.12) is used)} \\ &\Leftrightarrow r \in T^n \mathcal{R}_k. \end{aligned}$$

We thus obtain (A.13).

$$\begin{aligned} r \in \mathcal{R}_{2n-k} &\Leftrightarrow r = I_{2n-k} r \qquad \text{((A.12) is used)} \\ &= T^{n-k} \circ I_k \circ T^{k-n} r \qquad \text{((A.9) and (A.11) are used)} \\ &\Leftrightarrow I_k \circ (T^{k-n} r) = T^{k-n} r \\ &\Leftrightarrow T^{k-n} r \in \mathcal{R}_k \qquad \text{(A.12) is used)} \qquad (A.16) \\ &\Leftrightarrow I_k T^{k-n} r \in I_k \mathcal{R}_k = \mathcal{R}_k \qquad \text{((A.12) is used)} \\ &\Leftrightarrow I_n r \in \mathcal{R}_k \qquad \text{((A.11) is used)} \\ &\Leftrightarrow r \in I_n \mathcal{R}_k \qquad \text{((A.8) is used).} \end{aligned}$$

We thus obtain (A.14).

In (A.13), by substituting 0 or 1 to k, we get

$$\mathcal{R}_{2n} = T^n \mathcal{R}_0 \tag{A.17}$$

$$\mathcal{R}_{2n+1} = T^n \mathcal{R}_1. \tag{A.18}$$

These are the non-trivial relations used in section 2.

The intersection of the sets $\mathcal{R}_i$ and $\mathcal{R}_j$ includes the periodic points with the period $n = |i - j|$, since

$$\begin{aligned} \boldsymbol{r} \in \mathcal{R}_i \cap \mathcal{R}_j &\Leftrightarrow I_i \boldsymbol{r} = \boldsymbol{r} \qquad \text{and} \qquad I_j \boldsymbol{r} = \boldsymbol{r} \\ &\Leftrightarrow I_i \boldsymbol{r} = I_j \boldsymbol{r} \\ &\Leftrightarrow T^i \circ I_0 \boldsymbol{r} = T^j \circ I_0 \boldsymbol{r} \\ &\Leftrightarrow I_0 \circ T^{i-j} \circ I_0 \boldsymbol{r} = \boldsymbol{r} \\ &\Leftrightarrow T^{j-i} \boldsymbol{r} = \boldsymbol{r} \\ &\Leftrightarrow \boldsymbol{r} : \text{a periodic point of the period } |i - j|. \end{aligned} \tag{A.19}$$

Therefore, we can determine the location of various periodic orbits by calculating the intersection $\mathcal{R}_i \cap \mathcal{R}_j$ for $i, j \in Z$. However, we note that some periodic orbits cannot be captured by this method.

References

[1] Cvitanović P (ed) 1992 *Chaos* **2** 1–158

[2] Ruelle D 1978 *Statistical Mechanics, Thermodynamic Formalism* (Reading, MA: Addison-Wesley)

[3] Gutzwiller M C 1990 *Chaos in Classical and Quantum Mechanics* (New York: Springer)

[4] Hannay J H and Berry M V 1980 *Physica* D **1** 267
Keating J P 1991 *Nonlinearity* **4** 277, 309

[5] Balazs N L and Voros A 1987 *Europhys Lett.* **4** 1089; 1989 *Ann. Phys.* **190** 190
Saraceno M 1990 *Ann. Phys.* **199** 37
Ozorio de Almeida A M and Saraceno M 1991 *Ann. Phys.* **210** 1
O'Conner P W and Tomsovic S 1991 *Ann. Phys.* **207** 218

[6] Eckhardt B 1987 *J. Phys. A: Math. Gen.* **20** 5971

[7] Gaspard P and Rice S A 1989 *J. Chem. Phys.* **90** 2225, 2242, 2255; 1989 *J. Chem. Phys.* **91** E3279

[8] Gaspard P and Alonso Ramirez D 1992 *Phys. Rev.* A **45** 8383

[9] Cvitanović P and Eckhardt B 1989 *Phys. Rev. Lett.* **63** 823

[10] Birkhoff G D 1950 *Collected Mathematical Papers* vol I (Providence, RI: American Mathematical Society) p 727; vol II, pp 412, 489, 668, 718; 1972 *Dynamical Systems* (Providence, RI: American Mathematical Society) p 186
Piña E and Lara L J 1987 *Physica* **26D** 369
Richter P H, Scholtz H-J and Wittek A 1990 *Nonlinearity* **3** 45

[11] Jung C and Richter P H 1990 *J. Phys. A: Math. Gen.* **23** 2847

[12] Morita T 1991 *Trans. Am. Math.* **325** 819

[13] Troll G and Smilansky U 1992 *Physica* **35D** 34; 1991 *Physica* **50D** 276; 1992 *Nonlinearity* **5** 1151; 1993 Formal languages in dynamical systems *Preprint*; 1993 *Chaos* **3** 459

[14] Hansen K T 1992 *Chaos* **2** 71; 1993 *Nonlinearity* **6** 753,770; 1992 Symbolic dynamics: III. Bifurcation in billiards and smooth potentials *Preprint*

[15] Harayama T and Shudo A 1992 *J. Phys. A: Math. Gen.* **25** 4595

[16] Sano M M 1994 in preparation

[17] Hansen K T 1993 Symbolic dynamics in chaotic systems *PhD Thesis* University of Oslo